Available online at www.sciencedirect.com
SCIENCE DIRECT®
Journal of Sound and Vibration 266 (2003) 1117–1129
JOURNAL OF SOUND AND VIBRATION
www.elsevier.com/locate/jsvi

Letter to the Editor

Influence of suspension damper asymmetry on vehicle vibration response to ground excitation

C. Rajalingham, S. Rakheja*

Concave Research Center, Department of Mechanical Engineering, Concordia University, Montreal, Que., Canada H3G 1M8

Received 11 April 2002; accepted 15 December 2002

1. Introduction

The dampers employed in automotive suspension are mostly designed to yield asymmetric damping characteristics in compression and rebound in order to achieve a better compromise between ride, road-holding, handling and control performance of the vehicle [1]. Owing to considerably higher wheel velocity in the upward direction, when compared to that in the downward direction, the dampers provide significantly higher damping force in rebound. The non-linear and asymmetric damping properties of shock absorbers have been widely characterized in terms of hysteresis and peak force–peak velocity characteristics [2,3]. A number of analytical models based upon fluid flows through damper orifices and valves, and semi-empirical formulations have been developed to characterize the asymmetric force–velocity characteristics [4,5]. Since these models require prior knowledge of various coefficients to be derived from the measured data for a specific damper, their applications have been limited for analysis of vehicle ride and handling.

Majority of the analyses involving road vehicle ride dynamics, road-holding and handling and control performance therefore consider either linear or piece-wise linear and symmetric damping properties, assuming negligible contributions due to asymmetry, hysteresis and gas spring effect [6]. Analytical and experimental investigations performed on high-performance dampers with asymmetric properties in compression and rebound reveal considerable downward shift in the mean position of the sprung mass, referred to as 'packing or jacking down' [7]. This phenomenon has been attributed to asymmetric nature of the dampers. The potential energy stored in the suspension spring during compression is dissipated during extension under higher damping thereby reducing the rate of rebound motion and causing a downward shift in the operating equilibrium position of the vehicle sprung mass.

*Corresponding author. Tel.: +514-848-3148; fax: +514-848-8635.

0022-460X/03/$ - see front matter
doi:10.1016/S0022-460X(03)00054-3

While a few studies have considered asymmetric suspension damping properties within the vehicle models, the effect of asymmetric damping on the downward shift is not explored [8,9]. These studies involved the analyses of either acceleration response under random road excitations or suspension deflection under bump type of excitation, where the downward shift in the sprung mass deflection does not become apparent. The downward shift in sprung mass position can affect the vehicle ride and handling due to variations in the ride height. In this study, the effect of asymmetric damping on the sprung mass position is investigated through analysis of a two-degrees-of-freedom (2-d.o.f.) quarter-vehicle model. The suspension damping is represented by force–velocity characteristics asymmetric in compression and rebound. The analysis is performed under harmonic displacement excitation and the results are presented to enhance an understanding of the mechanism associated with downward shifting of the sprung mass.

2. Theory

Fig. 1 illustrates a 2-d.o.f. quarter-vehicle model. The vehicle body and chassis mass is represented by the sprung mass m_2, which is supported by the axle and the tired-wheel unsprung mass m_1 through a linear spring and a damper. The tire is characterized by a linear spring and a viscous damper, assuming point contact with the road surface. Assuming small seal friction and gas spring force, the force generated by the shock absorber is characterized by the asymmetric force–velocity shown in Fig. 2. A shock absorber in general yields force limiting at higher velocities through the use of either single or multi-stage pressure limiting valves [3,9]. The peak force–peak velocity characteristics, therefore, yield a high damping coefficient at a low velocity, which reduces to a considerably lower value at a higher velocity. The transition from high to low damping coefficient occurs at a preset velocity. The force-limiting property of the damper is neglected in this study in order to study the effect of damping asymmetry alone.

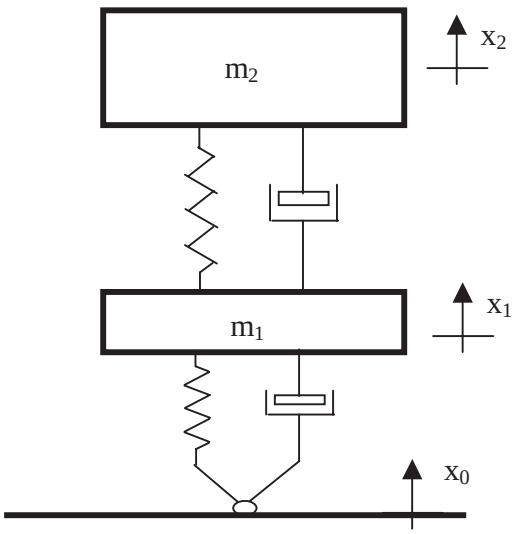

Fig. 1. 2-d.o.f. quarter-vehicle model.

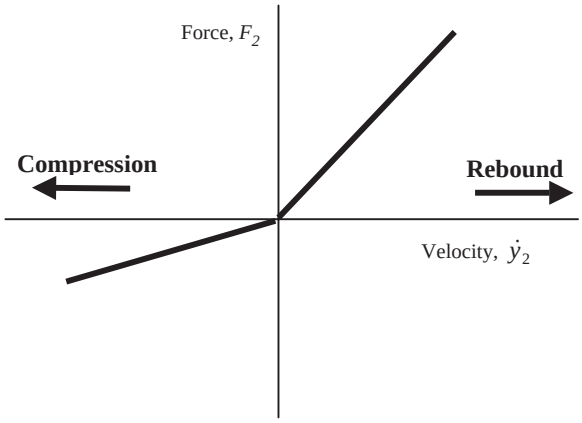

Fig. 2. Idealized asymmetric force–velocity characteristics of a damper.

The displacement co-ordinates x_1 and x_2 of the masses, shown in Fig. 1, for the ground displacement x_0, are not convenient to handle the non-linear force–velocity relationship of the suspension damper. The extensions y_1 and y_2 of the springs, defined by $y_1 = x_1 - x_0$ and $y_2 = x_2 - x_1$ are the convenient intermediate co-ordinates for the present study. For dynamic analysis, the force–velocity relationship of the suspension damper can be approximated by a sequence of connected straight-line segments. This relationship is further simplified for the present analysis as

$$F_2^{(c)}(\dot{y}_2) = \begin{cases} c_2^{(-)}\dot{y}_2, & \dot{y}_2 \leqslant 0, \\ c_2^{(+)}\dot{y}_2, & \dot{y}_2 \geqslant 0. \end{cases} \tag{1}$$

Since $F_2^{(c)}(0) = 0$, the value of $F_2^{(c)}$ at $\dot{y}_2 = 0$ can be calculated from any one of the two expressions in Eq. (1). Here, $\dot{y}_2 \leqslant 0$ represents the compressive motion of the damper, whereas $\dot{y}_2 \geqslant 0$ denotes its rebounding motion. For a time interval within which $\dot{y}_2$ maintains the same sign, the system can be treated like a locally linear one, and the exact solution of the equations of motion can be constructed in terms of the initial conditions. This exact solution is valid only for the time interval within which $\dot{y}_2$ maintains the same sign. The validity of the exact solution can be extended until $\dot{y}_2$ becomes zero. The exact solution at the end of this time interval can be used as the initial condition to construct the exact solution for the subsequent time interval. Thus, a single parameter c_2 can be used to represent both $c_2^{(-)}$ and $c_2^{(+)}$ in the presentation of the theory. The equations of motion of the masses can thus be expressed as

$$(m_1\ddot{y}_1 + c_1\dot{y}_1 + k_1y_1) - (c_2\dot{y}_2 + k_2y_2) = -m_1\ddot{x}_0, \tag{2}$$

$$m_2\ddot{y}_1 + (m_2\ddot{y}_2 + c_2\dot{y}_2 + k_2y_2) = -m_2\ddot{x}_0. \tag{3}$$

It is possible to express Eqs. (2) and (3) as a system of four first order differential equations and solve them numerically using Runge–Kutta algorithm. However, the whipping up of the complementary functions by damper non-linearity is expected to introduce numerical inaccuracies in the computation. Laplace transform method is used to solve the governing equations in the present study.

In order to apply the Laplace transform method to this globally non-linear system, it is necessary to define a local time t, corresponding to the global time τ, by the relation $t = \tau - \tau_{in}$.

Here, τ_{in} is the global time at the commencement of the time interval under investigation. The ground displacement x_0 for this analysis is taken as $\delta_0 \sin \omega(t+\tau_{in})$. For the chosen type of damper non-linearity, Eqs. (1)–(3) indicate that the parameter δ_0 can be used as a standard length to non-dimensionalize the variables y_1 and y_2. With the understanding that the variables y_1, y_2 and x_0 are non-dimensionalized using the standard length δ_0, the value of δ_0 can be set to unity without any loss of generality. For Laplace transform analysis, it is convenient to assign f for the variable $-\ddot{x}_0$ on RHS of Eqs. (2) and (3). Thus, the expression for f becomes $\omega^2 \sin \omega(t+\tau_{in})$. Introducing two additional variables $y_3 = \dot{y}_1$ and $y_4 = \dot{y}_2$, Eqs. (2) and (3) can be Laplace transformed as

$$\begin{bmatrix} m_1 s^2 + c_1 s + k_1 & -c_2 s - k_2 \\ m_2 s^2 & m_2 s^2 + c_2 s + k_2 \end{bmatrix} \begin{bmatrix} Y_1 \\ Y_2 \end{bmatrix} = y_{10} \begin{bmatrix} m_1 s + c_1 \\ m_2 s \end{bmatrix} + y_{20} \begin{bmatrix} -c_2 \\ m_2 s + c_2 \end{bmatrix} + y_{30} \begin{bmatrix} m_1 \\ m_2 \end{bmatrix} + y_{40} \begin{bmatrix} 0 \\ m_2 \end{bmatrix} + F \begin{bmatrix} m_1 \\ m_2 \end{bmatrix}. \tag{4}$$

Here, the coefficient y_{i0} on RHS indicates the initial values of the variables y_i. In the present convention, the majuscule variable symbol represents Laplace transform of the corresponding variable denoted by the minuscule. The variable F in Eq. (4) is the Laplace transform of the variable $f = \omega^2 \sin \omega\tau_{in} \cos \omega\, t + \omega^2 \cos \omega\tau_{in} \sin \omega\, t$. The determinant of the coefficient matrix in Eq. (4) can be simplified as

$$\Delta = m_1 m_2 s^4 + \{(m_1 + m_2)c_2 + m_2 c_1\} s^3 + \{(m_1 + m_2)k_2 + m_2 k_1 + c_1 c_2\} s^2 + (c_1 k_2 + c_2 k_1) s + k_1 k_2. \tag{5}$$

The roots of the characteristic equation, $\Delta = 0$ of the governing differential equations, determine the complimentary part of the solution. The quartic expression for Δ, given in Eq. (5), can be factorized into two quadratic factors with real coefficients. From the roots of these quadratic factors, the four natural functions $\psi_k(t)$ of the complimentary part of the solution can be determined. Since c_2 can take either of the two values $c_2^{(+)}$ or $c_2^{(-)}$, depending on the sign of $\dot{y}_2$, the above-mentioned procedure yields two sets four natural functions corresponding to the two types of motions of the suspension damper. From Eq. (4), the solutions for the transformed functions Y_1 and Y_2 can be simplified as

$$\begin{bmatrix} Y_1 \\ Y_2 \end{bmatrix} = y_{10} \begin{bmatrix} A_{11} \\ A_{21} \end{bmatrix} + y_{20} \begin{bmatrix} A_{12} \\ A_{22} \end{bmatrix} + y_{30} \begin{bmatrix} A_{13} \\ A_{23} \end{bmatrix} + y_{40} \begin{bmatrix} A_{14} \\ A_{24} \end{bmatrix} + F \begin{bmatrix} A_{13} \\ A_{23} \end{bmatrix}, \tag{6}$$

where

$$A_{11} = \{m_1 m_2 s^3 + \{(m_1 + m_2)c_2 + m_2 c_1\} s^2 + \{(m_1 + m_2)k_2 + c_1 c_2\} s + c_1 k_2\}/\Delta,$$

$$A_{12} = m_2 k_2 s/\Delta, \quad A_{13} = \{m_1 m_2 s^2 + (m_1 + m_2)c_2 s + (m_1 + m_2)k_2\}/\Delta,$$

$$A_{14} = \{m_2 c_2 s + m_2 k_2\}/\Delta, \quad A_{21} = m_2 k_1 s/\Delta,$$

$$A_{22} = \{m_1m_2s^3 + \{(m_1 + m_2)c_2 + m_2c_1\}s^2 + \{m_2k_1 + c_1c_2\}s + c_2k_1\}/\Delta,$$

$$A_{23} = \{m_2c_1s + m_2k_1\}/\Delta \quad \text{and} \quad A_{24} = \{m_1m_2s^2 + m_2c_1s + m_2k_1\}/\Delta.$$

Since $y_3 = \dot{y}_1$ and $y_4 = \dot{y}_2$, Laplace transform of the velocities of the masses can be expressed as $Y_3 = sY_1 - y_{10}$ and $Y_4 = sY_2 - y_{20}$. Using Eq. (5), the expressions for Y_3 and Y_4 can be obtained as

$$\begin{bmatrix} Y_3 \\ Y_4 \end{bmatrix} = y_{10}\begin{bmatrix} A_{31} \\ A_{41} \end{bmatrix} + y_{20}\begin{bmatrix} A_{32} \\ A_{42} \end{bmatrix} + y_{30}\begin{bmatrix} A_{33} \\ A_{43} \end{bmatrix} + y_{40}\begin{bmatrix} A_{34} \\ A_{44} \end{bmatrix} + F\begin{bmatrix} A_{33} \\ A_{43} \end{bmatrix}, \tag{7}$$

where

$$A_{31} = \{-m_2k_1s^2 - c_2k_1s - k_1k_2\}/\Delta, \quad A_{32} = m_2k_2s^2/\Delta,$$

$$A_{33} = \{m_1m_2s^3 + (m_1 + m_2)c_2s^2 + (m_1 + m_2)k_2s\}/\Delta, \quad A_{34} = \{m_2c_2s^2 + m_2k_2s\}/\Delta,$$

$$A_{41} = m_2k_1s^2/\Delta, \quad A_{42} = \{-(m_1 + m_2)k_2s^2 - c_1k_2s - k_1k_2\}/\Delta,$$

$$A_{43} = \{m_2c_1s^2 + m_2k_1s\}/\Delta, \quad A_{44} = \{m_1m_2s^3 + m_2c_1s^2 + m_2k_1s\}/\Delta.$$

In the present nomenclature, Eqs. (6) and (7) can be expressed in its abridged form as $Y_i = \sum_{j=1}^{4} A_{ij}y_{j0} + A_{i3}F$. The solution of the equations can be obtained by taking the inverse Laplace transform of the four variables Y_i. Since the expressions of the coefficient variables A_{ij}, given in Eqs. (6) and (7) are proper rational functions of s, they can be expressed as partial fraction form using the roots of the characteristic equation $\Delta = 0$. The inverse transform of A_{ij} can therefore be expressed in terms of the natural functions as

$$a_{ij}(t) = \sum_{k=1}^{4} \alpha_{ijk}\psi_k(t). \tag{8}$$

It can be observed that the coefficients α_{ijk} in Eq. (8) are independent of the initial conditions and the forcing frequency. Since $f = \omega^2 \sin\omega\tau_{in} \cos\omega t + \omega^2 \cos\omega\tau_{in} \sin\omega t$, the remaining component $A_{i3}F$ in the expression for Y_i can be expressed as $A_{i3}F = \omega^2 \sin\omega\tau_{in}P_i + \omega^2 \cos\omega\tau_{in}Q_i$. As before, the partial fraction expression can be used to invert the functions $P_i = A_{i3}s/(s^2 + \omega^2)$ and $Q_i = A_{i3}\omega/(s^2 + \omega^2)$ as

$$p_i(t) = \sum_{k=1}^{4} \beta_{ik}\psi_k(t) + \beta_{i5}\cos\omega t + \beta_{i6}\sin\omega t, \tag{9}$$

$$q_i(t) = \sum_{k=1}^{4} \gamma_{ik}\psi_k(t) + \gamma_{i5}\cos\omega t + \gamma_{i6}\sin\omega t. \tag{10}$$

Here, the coefficients β_{ik} and γ_{ik} in Eqs. (9) and (10) are independent of the initial conditions.

By taking the inverse transform of $Y_i = \sum_{j=1}^{4} A_{ij}y_{j0} + A_{i3}F$, the solution for y_i can be written as $y_i = \sum_{j=1}^{4} y_{j0}a_{ij}(t) + \omega^2 \sin\omega\tau_{in}p_i(t) + \omega^2 \cos\omega\tau_{in}q_i(t)$. Using Eqs. (8)–(10), the solution can be

further simplified in terms of the coefficients α_{ijk}, β_{ik} and γ_{ik} as

$$y_i = \sum_{k=1}^{4} \lambda_{ik}\psi_k(t) + \lambda_{i5}\cos\omega t + \lambda_{i6}\sin\omega t, \tag{11}$$

where

$$\lambda_{ik} = \begin{cases} \sum_{j=1}^{4} \alpha_{ijk}y_{j0} + \beta_{ik}\omega^2 \sin\omega\tau_{in} + \gamma_{ik}\omega^2\cos\omega\tau_{in}, & k = 1,4, \\ \beta_{ik}\omega^2\sin\omega\tau_{in} + \gamma_{ik}\omega^2\cos\omega\tau_{in}, & k = 5,6. \end{cases}$$

The exact solution, given in Eq. (11), is valid for any time interval within which $\dot{y}_2$ maintains the same sign. If $\dot{y}_2$ is zero at the beginning of the time interval, the value of c_2 for the subsequent motion can be selected from the sign of $\ddot{y}_2$. For this purpose, explicit expression for $\ddot{y}_2$ can be obtained from Eqs. (2) and (3) as

$$\ddot{y}_2 = \{(c_1\dot{y}_1 + k_1y_1) - (1 + m_1/m_2)(c_2\dot{y}_2 + k_2y_2)\}/m_1. \tag{12}$$

In a theoretical sense, the system response can be reconstructed as a sequential arrangement of the exact solutions for compressive ($\dot{y}_2 \leqslant 0$) and rebounding ($\dot{y}_2 \geqslant 0$) motions of the damper. At the beginning and the end of these two types of motions, the velocity $\dot{y}_2$ is zero. Further, the final values of the solutions for y_1, y_2, y_3 and y_4 of one type of motion can be used as the respective initial conditions for the subsequent motion. The presence of exponential functions in the expressions of natural functions can introduce numerical difficulties in implementing the above solution method. Controlling the time interval of the computation can circumvent such numerical difficulties.

For approximate analysis, the dynamical system can be linearized by replacing the non-linear damper with an equivalent viscous damper that dissipates the same amount of energy during vibration. Assuming the velocity $\dot{y}_2$ as $\omega\delta_{2a}\cos(\omega\tau + \phi)$, the energy dissipation within one cycle can be estimated as $(\pi/2)(c_2^{(+)} + c_2^{(-)})\omega\delta_{2a}^2$ leading to the equivalent damping coefficient as

$$c_2^{(eq)} = (c_2^{(+)} + c_2^{(-)})/2. \tag{13}$$

However, the solutions of the linearized system equations cannot be expected to reveal special features, such as the shift in the mean positions of the sprung mass.

3. Results and discussion

The system parameters for the quarter-car model are considered as follows: $m_1 = 40\,\text{kg}$, $m_2 = 240\,\text{kg}$, $c_1 = 50\,\text{N s/m}$, $c_2^{(-)} = 515\,\text{N s/m}$, $c_2^{(+)} = 2750\,\text{N s/m}$, $k_1 = 160\,\text{kN/m}$ and

Table 1
Roots of characteristic equations for compressive and rebounding motions

Type of motion		Compressive, $\dot{y}_2 < 0$	Rebounding, $\dot{y}_2 > 0$
First pair	Real part	−0.88846740	−5.6312991
	Imaginary part	7.7499996	6.4808843
Second pair	Real part	−8.0316715	−38.986756
	Imaginary part	69.315458	49.996050

$k_2 = 160\,\mathrm{kN/m}$ [10]. The roots of the characteristic equation $\Delta = 0$ for the compressive and rebounding motions of the shock absorber are tabulated in Table 1. For the present analysis, the ground displacement $x_0 = \sin\omega\tau$ is imposed on the system at $\tau = 0$. Assuming the system to be at rest for $\tau < 0$, the initial values of the four system variables can be expressed as $y_{10} = 0$, $y_{20} = 0$, $y_{30} = -\omega$ and $y_{40} = 0$. Since the initial velocity $\dot{y}_2$ is zero, Eq. (12) is used to establish the sign of $\ddot{y}_2$ as negative. Thus, the damper initially undergoes a compressive motion, and $c_2 = c_2^{(-)}$.

Table 1 indicates that the largest frequency components in the natural functions associated with the compressive and rebounding motions are 69.3 and 50 rad/s, respectively, attributed to resonances of the unsprung mass. The resonant frequencies of both the sprung and unsprung masses tend to be lower in rebound than those in compression. In addition, the response will have the forced vibration components at excitation frequency ω. A nominal time step of $t_n = 0.1\,\pi/\max(69.3, 50.0, \omega)$ s is chosen for the numerical computation. Whenever a change in the sign of $\dot{y}_2$ is encountered the time step is systematically reduced to ensure $\dot{y}_2 \approx 0$ at the end of the step. The error in the time step is kept below $10^{-15}t_n$. Computations are carried out in a 16-bit computer in quadruple precision.

A typical set of solutions for displacements and velocities of the unsprung and sprung masses corresponding to the ground excitation at 2.0 Hz are shown in Figs. 3–6. The linearized system solutions are also included for comparison. These linearized solutions are obtained by replacing $c_2^{(+)}$ and $c_2^{(-)}$ with $c_2^{(eq)}$. The displacement and velocity responses are normalized by using δ_0 and $\omega\delta_0$, and ωt is represented as the non-dimensional time. Fig. 4 indicates a significant difference between the non-linear and linear solutions for the sprung mass displacement. This downward shift in the mean position of the sprung mass is a phenomenon that cannot be explained by the linearized model. However, the displacement of the unsprung mass, shown in Fig. 3 does not exhibit this mean position shift. The velocity responses of the unsprung and sprung masses of the non-linear model differ only slightly from those of the linear system, as shown in Figs. 5 and 6, respectively.

It is desirable to understand the physical reason for the downward shift in the mean position of the sprung mass. The result shown in Fig. 4 indicates that the suspension spring displacement can be considered as a superposition of a vibrating component on a mean compression. This extension

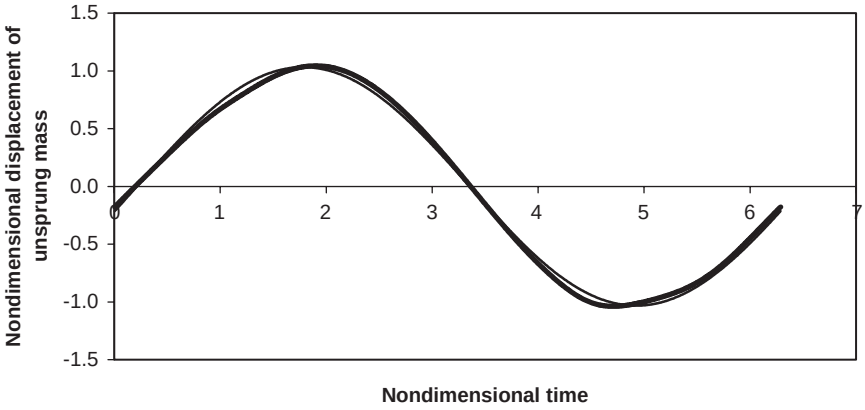

Fig. 3. Variation of the unsprung mass displacement response with time (——, linear; ——, non-linear).

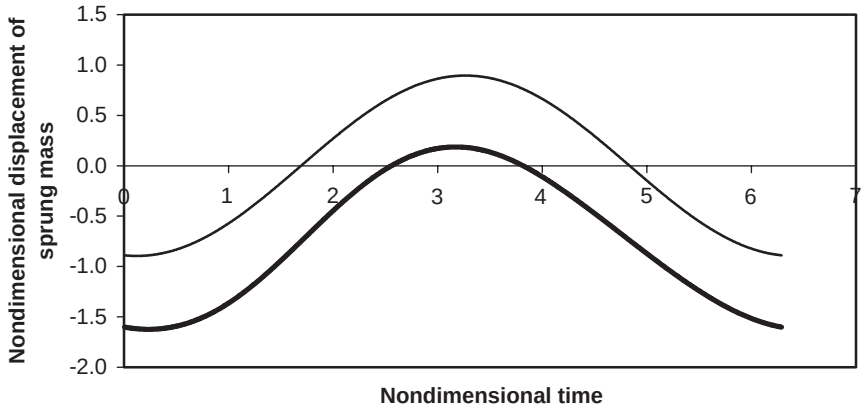

Fig. 4. Variation of the sprung mass displacement response with time (——, linear; ——, non-linear).

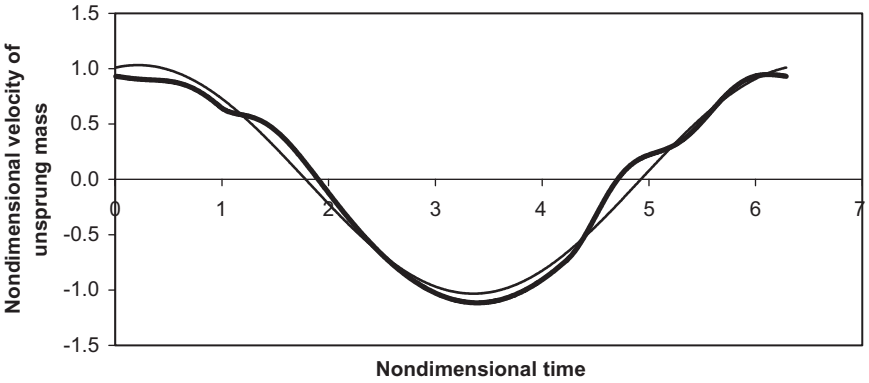

Fig. 5. Variation of the unsprung mass velocity with time (——, linear; ——, non-linear).

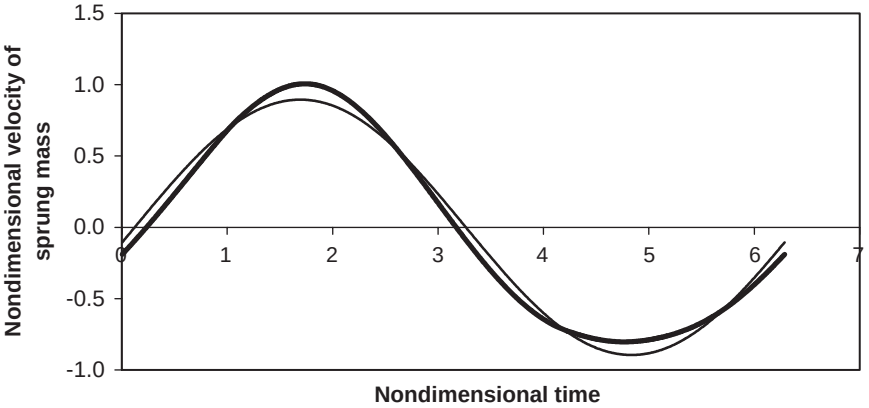

Fig. 6. Variation of the sprung mass velocity with time (——, linear; ——, non-linear).

can be approximated as

$$y_2 \approx \delta_{2m} + \delta_{2a}\sin(\omega\tau + \phi). \tag{14}$$

The mean value of the force developed by the suspension components can be estimated as

$$\left\{\int_0^{2\pi/\omega} k_2 y_2 \,\mathrm{d}\tau + \int_{(\pi/2-\phi)/\omega}^{(3\pi/2-\phi)/\omega} c_2^{(-)}\dot{y}_2 \,\mathrm{d}\tau + \int_{(3\pi/2-\phi)/\omega}^{(5\pi/2-\phi)/\omega} c_2^{(+)}\dot{y}_2 \,\mathrm{d}\tau\right\} \Big/ \left(\frac{2\pi}{\omega}\right),$$

which simplifies to $k_2\delta_{2m} + (c_2^{(+)} - c_2^{(-)})\delta_{2a}\omega/\pi$. Since, there is no shift in the mean position of the unsprung mass, as seen from Fig. 3, the magnitude of this mean force transmitted must be zero. Consequently, this no-mean-force concept may be used to estimate extension δ_{2m} of the suspension from the alternating component using the relation

$$\delta_{2m} = -\left\{(c_2^{(+)} - c_2^{(-)})\omega/\pi k_2\right\}\delta_{2a}. \tag{15}$$

The displacements of the masses, shown in Figs. 3 and 4, are periodic variations with a predominant constituent at the forcing frequency along with its harmonics. The displacement can be decomposed into a mean and an alternating component. Owing to the presence of higher harmonics in the alternating component, the root mean square (r.m.s.) value is used to quantify this component. The variations of the mean of the displacements of the sprung mass against the forcing frequency are shown in Fig. 7, and those in the alternating components of the sprung and unsprung masses are shown in Figs. 8 and 9, respectively. It can be observed, from Fig. 7, that the mean position shift of the sprung mass cannot be predicted using the linearized equations of motion. However, Figs. 8 and 9 indicate that the predictions of the alternating components from the linearized system equations are reasonably accurate for design calculations.

It is interesting to investigate whether Eq. (15) can be used to estimate the mean position shift of the sprung mass from the solutions of the linearized equations. The variations of the mean of the extension of the suspension springs, shown in Fig. 10, and those in alternating components of unsprung as well as sprung masses (Figs. 11 and 12), are needed for such verification. Here,

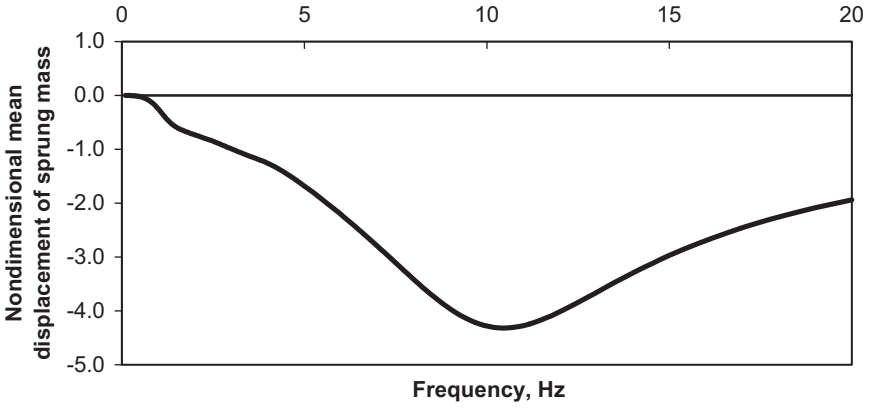

Fig. 7. Variations of the mean displacement response of the sprung mass with frequency (——, linear; ——, non-linear).

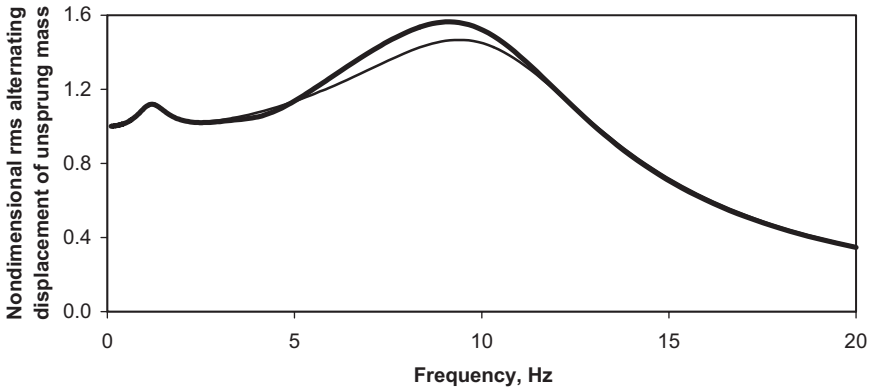

Fig. 8. Variations of the alternating component of the displacement response of the unsprung mass with frequency (——, linear; ——, non-linear).

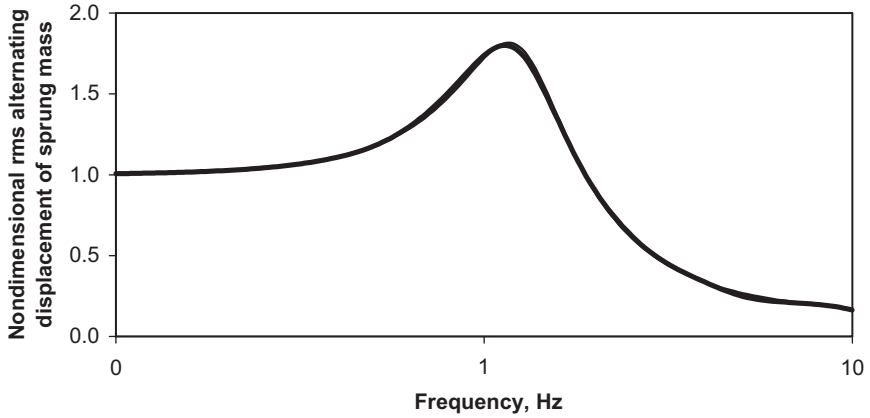

Fig. 9. Variations of the alternating component of the displacement response of the sprung mass with frequency (——, linear; ——, non-linear).

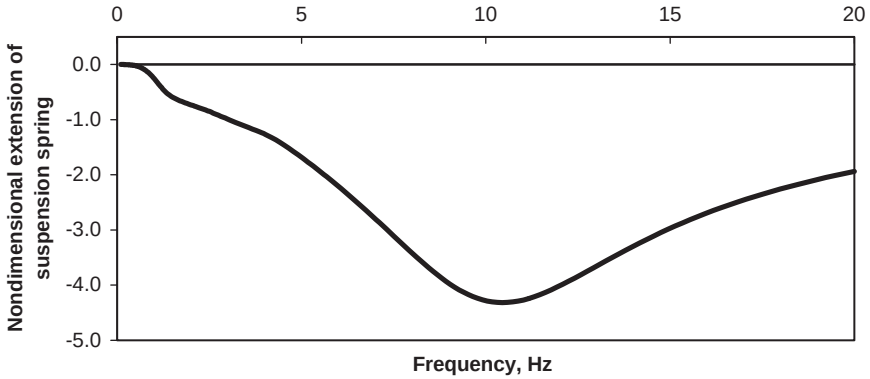

Fig. 10. Variations of the mean value of the suspension spring extension with frequency (——, linear; ——, non-linear).

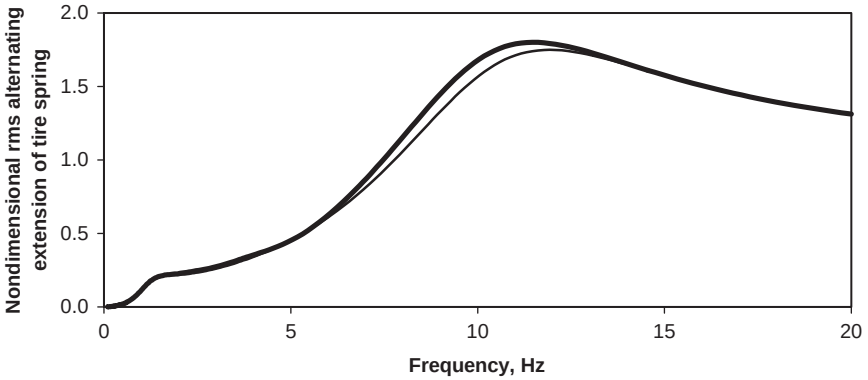

Fig. 11. Variations of the alternating component of the tire spring extension with frequency (——, linear; ——, non-linear).

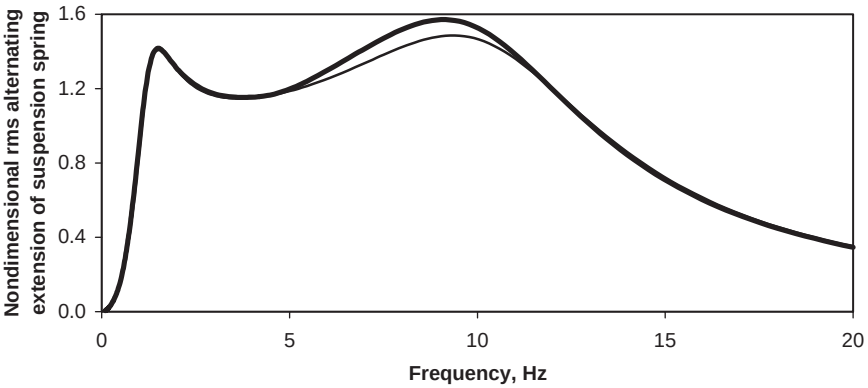

Fig. 12. Variations of the alternating component of the suspension spring extension with frequency (——, linear; ——, non-linear).

Figs. 11 and 12 indicate that the predictions of the alternating components of these spring extensions from the linearized equations are reasonably accurate for design calculations. Further, Fig. 10 indicates that the mean position shift of the sprung mass is due to the compression of the suspension spring.

The variation of the ratio of the mean to alternating component of the suspension spring extension against the forcing frequency is shown in Fig. 13. As expected from Eq. (15), the variation shown in Fig. 13 is approximately a straight line with slope $-0.27953\,\mathrm{Hz}^{-1}$. For this approximately linear variation, Eq. (15) predicts its slope as $-2(c_2^{(+)} - c_2^{(-)})/k_2$, which for the present data simplifies to $-0.27938\,\mathrm{Hz}^{-1}$. Further, this approximate solution for the mean component of the suspension spring extension can be used to assign the approximate initial conditions for the numerical simulation of non-linear equations. Such an informed choice of initial conditions can be used to control fluctuations in the natural function

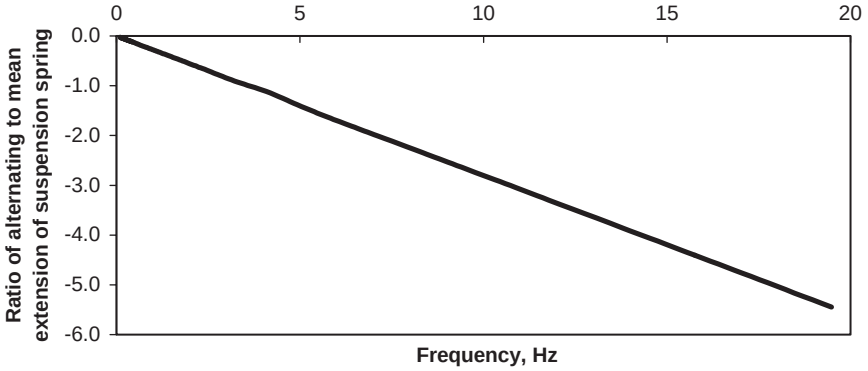

Fig. 13. Variations of the ratio of alternating component to mean value of the suspension spring extension with frequency.

components during convergence, which in turn will be helpful in numerical simulation of non-linear equations.

4. Conclusions

The influence of suspension damper asymmetry on the vehicle vibration response due to ground excitation is analyzed using the well-known quarter car model. The non-linear suspension damper is considered to have different damping coefficients for compressive and rebounding motions of the suspension. The exact solutions to these two types of motions are obtained using Laplace transformation method. These exact solutions are used to reconstruct the motions of the non-linear system. The solution of the non-linear system equations indicates that the suspension damping asymmetry introduces a downward shift in the mean position of the sprung mass in addition to the vibratory response, which conforms with the 'packing down' phenomenon. However, the response of the unsprung mass does not exhibit such a mean position shift. The mean position shift in the sprung mass is due to the mean compression in the suspension spring caused by the force imbalance in the suspension damper during vibration. The concept that the mean value of the damper force is zero, is used to express the mean compression of the suspension spring in terms of the associated alternating component. The accuracy of this zero-mean-force concept for the determination of the mean compression of the suspension spring is found to be satisfactory.

The system equations can be linearized by replacing the non-linear damper with an equivalent linear one on the basis of dissipated energy similarity. The linearized equations are found to predict the vibratory component of the response to satisfactory accuracy. However, the presence of the mean position shift of the sprung mass cannot be predicted. The mean position shift of the sprung mass can be estimated from the alternating component solutions of the linearized equations using the zero-mean-force concept, which is reasonably accurate for design calculations. Such an improved solution can be efficiently used to formulate the initial conditions for numerical simulation of the non-linear system equations.

References

[1] W.F. Milliken, D.L. Milliken, Race Car Vehicle Dynamics, Society of Automotive Engineers, Troy, MI, 1995.
[2] R. Karadayi, G.Y. Masada, A nonlinear shock absorber model, Proceedings of the ASME Winter Annual Meeting, Anaheim, CA, 1986, pp. 149–165.
[3] P. Causeman, Automotive Shock Absorbers, Verlag Moderne Industrie, Lansberg, Germany, 2000.
[4] L. Segal, H.H. Lang, The mechanics of automotive dampers at high stroking frequencies, Vehicle System Dynamics, IAVSD Extensive Summaries, 1981, pp. 82–85.
[5] K. Reybrouck, A nonlinear parametric model of an automobile shock absorber, Society of Automotive Engineers, Paper No. 940869, 1994.
[6] Z. Jiang, D.A. Streit, M. El-Gindy, Heavy vehicle ride comfort: Literature review, Heavy Vehicle Systems, International Journal of Vehicle Design 8(3/4) (2001) 258–284.
[7] B. Warner, An Analytical and Experimental Investigation of High Performance Suspension Dampers, Ph.D. Thesis, Concordia University, Montreal, 1996.
[8] C. Kimim, P.I. Ro, H. Kim, Effect of suspension structure on equivalent suspension parameters, Proceedings of the Institute of Mechanical Engineers, Journal of Automobile Engineering 213(D5) (1999) 457–470.
[9] S. Rakheja, A.K.W. Ahmed, X. Yang, C. Guerette, Optimal suspension damping for improved driver- and road-friendliness of urban buses, Transactions of Society of Automotive Engineers, Journal of Commercial Vehicles 108 (2) (1999) 523–534.
[10] A. Ahmed, S. Rakheja, An equivalent linearization technique for frequency response analysis of asymmetric dampers, Journal of Sound and Vibration 153 (3) (1992) 537–542.